NANO LETTERS

Letter

pubs.acs.org/NanoLett

Tuning Electron Transfer Rates through Molecular Bridges in Quantum Dot Sensitized Oxides

Hai Wang,[†,‡] Erik R. McNellis,[†] Sachin Kinge,[*,§] Mischa Bonn,[†] and Enrique Cánovas[*,†,∥]

[†]Max Planck Institute for Polymer Research, Ackermannweg 10, 55128 Mainz, Germany

[‡]Graduate School Material Science in Mainz, University of Mainz, Staudingerweg 9, 55099 Mainz, Germany

[§]Materials Research and Development, Toyota Europe, Hoge Wei 33, B-1930 Zaventem, Belgium

[∥]FOM Institute for Atomic and Molecular Physics, Science Park 104, 1098 XG Amsterdam, The Netherlands

Supporting Information

ABSTRACT: Photoinduced electron transfer processes from semiconductor quantum dots (QDs) molecularly bridged to a mesoporous oxide phase are quantitatively surveyed using optical pump−terahertz probe spectroscopy. We control electron transfer rates in donor−bridge−acceptor systems by tuning the electronic coupling strength through the use of *n*-methylene (SH−$[CH_2]_n$−COOH) and *n*-phenylene (SH−$[C_6H_4]_n$−COOH) molecular bridges. Our results show that electron transfer occurs as a nonresonant quantum tunneling process with characteristic decay rates of β_n = 0.94 ± 0.08 and β_n = 1.25 per methylene and phenylene group, respectively, in quantitative agreement with reported conductance measurements through single molecules and self-assembled monolayers. For a given QD donor−oxide acceptor separation distance, the aromatic *n*-phenylene based bridges allow faster electron transfer processes when compared with *n*-methylene based ones. Implications of these results for QD sensitized solar cell design are discussed.

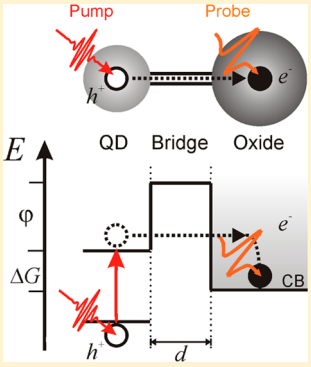

KEYWORDS: *Electron transfer, Marcus theory, molecular electronics, donor−bridge−acceptor, quantum dot sensitized solar cell, terahertz spectroscopy*

While metal oxides constitute robust and relatively cheap semiconductor materials that are finding increasing applications in optoelectronics, their band gaps are typically prohibitively wide for the generation of electron−hole pairs through the absorption of visible light. Several approaches have been developed to circumvent this drawback. Specifically, the sensitization of mesoporous oxides by semiconductor quantum dot (QD) nanocrystals represents a promising route for the development of low-cost solutions for energy production (i.e., in QD sensitized solar cells[1−3]) and storage (i.e., in photocatalyst for water splitting[4,5]). In a common approach for the sensitization of mesoporous oxide films with QDs, bifunctional molecular linkers are employed, for which each end of the molecule selectively anchors to the donor and acceptor, respectively.[6−9] This configuration has been termed a donor−bridge−acceptor system,[10] where the bridge imposes a barrier potential (φ) that has to be overcome in order for electron transfer (ET) to occur (see Figure 1). The barrier potential height is a direct measure of the donor−acceptor electronic coupling strength, and the ET rate is expected to decrease exponentially with both barrier height and bridge length.[10] Despite the apparent relevance for molecularly engineered novel and more efficient quantum dot-sensitized systems, little quantitative information exists regarding the role of the molecular bridge on the ET process. Existing studies have shown that the nature of the molecular bridge affects the ET processes[7−9] but are largely of a qualitative nature. This lack in our knowledge has been attributed to the challenge of quantifying ultrafast electron transfer processes in a noncontact fashion in these a priori highly heterogeneous systems.[10,11]

In previous work, we have demonstrated the unique potential of optical pump−terahertz (THz) probe (OPTP) measurements for interrogating ET processes on QD sensitized oxide films.[12,13] The strength of the technique relies on its ability to measure the complex (real and imaginary) photoconductivity of the sample after optical excitation with subpicosecond time resolution.[14] As long as charge carriers are confined within the QDs, the pump-induced real photoconductivity is zero; as soon as charges are transferred to the oxide, the carriers are free to move, and the real conductivity becomes finite. A gradual increase in the real conductivity with time after photoexcitation therefore directly and unambiguously reflects the ET processes taking place from the QD to the oxide. However, we have reported previously[12,13] that there is an additional, instantaneous contribution to the real conductivity upon photoexcitation due to free carriers populating QD aggregates. Here, we show how deliberate photo-oxidation of the sample allows us to separate out this parasitic signal to obtain pure ET kinetics.

Received: July 29, 2013
Revised: September 27, 2013
Published: October 7, 2013

   dx.doi.org/10.1021/nl402820v | *Nano Lett.* 2013, 13, 5311−5315

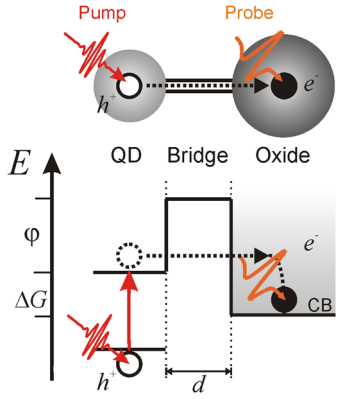

Figure 1. Principle of operation for time-resolved THz photoconductivity measurements and sketch of the energetics of the QD–bridge–oxide system. After selective absorption of a femtosecond optical pump pulse (red) by the QD, electron transfer through the molecular bridge to the oxide can occur (dashed arrow). Free electrons (e^-) populating the oxide conduction band (CB) can be selectively probed through their photoconductive response by a freely propagating THz pulse (orange). The excess energy ΔG of electrons in the QD excited state relative to the oxide conduction band (i.e., the driving force for electron transfer) triggers the electron transfer through a barrier potential of height φ and width d defined by the lowest unoccupied molecular orbital (LUMO) level of the molecular bridge.

As an example of the methodology, we show in Figure 2 the characteristic photo-oxidation OPTP dynamics for a sample

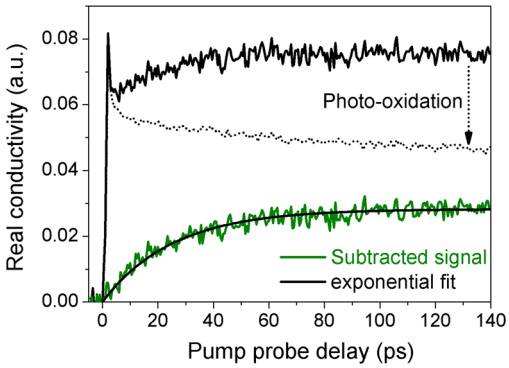

Figure 2. Characteristic evolution of the pump induced photoconductivity dynamics monitored by OPTP on CdSe QDs sensitizing SnO_2 connected by a HS–$[CH_2]_3$–COOH brigde, for the *unoxidized* sample (top black trace) and after 12 h exposure to air and 400 nm radiation (photo-oxidation process, black dotted trace). The green trace at the bottom is the difference between the two traces experiencing different degree of photo-oxidation and provides the kinetics of the real ET process. The black solid line is the corresponding single exponential fit.

consisting of ~3 nm diameter CdSe QDs sensitizing a mesoporous SnO_2 film by 4-mercaptobutyric acid (HS-$[CH_2]_3$-COOH). A detailed description of the sample preparation and measurement protocols are given in the Supporting Information. The solid black trace in Figure 2 is the time-resolved real conductivity signal for a sample preserved from photo-oxidation (prepared and measured under nitrogen environment). The real conductivity response of the sample is characterized by an instantaneous rise of the conductivity at time zero (attributed to photoconductivity within QD aggregates[12,13]) followed by a fast decay (due to trapping or recombination within those QD aggregates) and a picosecond time scale rise of the conductivity. Note that only the slow rise of the real conductivity signal (indicating an increasing population of free carriers in the oxide) is related to the ET process of interest.

Photo-oxidation of the sample is achieved by exposing the sample to air under identical optical excitation conditions (in this case 12 h with 400 nm pulses at 1 kHz at a fluence of 40 $\mu J/cm^2$, dotted black trace in Figure 2). Photo-oxidation of QDs causes quenching of QD luminescence,[15,16] as a result of the generation of electron traps in the QD surface. The generation of these traps also can prevent ET from QDs to the oxide phase,[13,17] which is apparent in our measurements from the disappearance of the time-dependent ingrowth of the photoconductivity upon photo-oxidation (Figure 2, dotted line). The instantaneous signal due to aggregated QDs remains, being a bulk signal that is less sensitive to the state of QDs at the surface of these aggregates. Hence, by comparing photoconductivity dynamics in the pristine sample with that in a photo-oxidized sample, for which ET is strongly suppressed, we can resolve unambiguously the ET component of interest. The green trace in Figure 2 is obtained by subtracting OPTP traces with different degree of oxidation (solid and dotted black traces in Figure 2). The resulting dynamics can be well-described by a single exponential function allowing for straightforward quantification of ET from the QD to the oxide.

Two important observations must be made here: (i) The inferred kinetics are independent of the degree of photo-oxidation for the two comparative measurements; (ii) while the parasitic signal can vary strongly between different samples, or even different spots on the same sample, our photo-oxidation protocol gives identical ET kinetics from sets of samples made with the same recipe (see the Supporting Information). It is remarkable to note that *monophasic* kinetics describe our measurements extremely well. This result implies that, following Marcus theory,[18] most of our QD sensitizers experience similar energetics (ΔG) and donor–acceptor electronic coupling strengths ($|H_{DA}|^2$), challenging the a priori intuition of ET heterogeneity for mesoporous systems. A detailed analysis of the degree of ET heterogeneity for different mesoporous oxides is in progress and will be reported elsewhere.

To study how the nature and length of the molecular bridge between QD donor and oxide acceptor affects ET rates, we investigate bridges based on *n*-methylene (HS–$[CH_2]_n$–COOH, n = 1, 3, 5, 7) and *n*-phenylene (HS–$[C_6H_4]_n$–COOH; n = 1, 2) backbones. The bridges form the connection between ~3 nm diameter CdSe QDs and SnO_2 nanoparticles, corresponding to a fixed driving force for ET of $\Delta G \sim 1.1$ eV;[18,19] see Figure 1. Figure 3a and b depicts the obtained ET kinetics for the two types of analyzed molecules; in both cases a slow-down of the ET rate with increasing bridge length is apparent. Also here, the ET kinetics can be described very well by single exponential functions (black solid lines in Figure 3a and b). Table 1 summarizes the extracted ET rates for all molecular bridges considered in this study, and the lengths of the corresponding gas-phase molecules as obtained through density-functional theory (DFT) calculations (see the Supporting Information). The kinetics of each sample was monitored within sufficiently large time windows to allow resolving the signal plateau (indicating that the ET process is complete). Only for the two largest *n*-methylene based bridges our

dx.doi.org/10.1021/nl402820v | Nano Lett. 2013, 13, 5311–5315

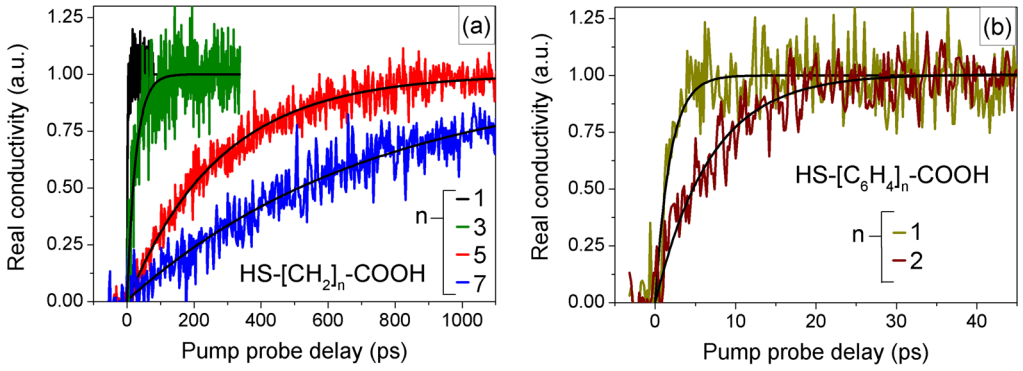

Figure 3. ET kinetics between ~3 nm CdSe QDs and SnO_2 through (a) *n*-methylene based bridges (HS−$[CH_2]_n$−COOH, with n = 1,3,5,7) and (b) *n*-phenylene based bridges (HS−$[C_6H_4]_n$−COOH, with n = 1, 2). Black lines depict single exponential fits.

Table 1. QD-Oxide ET Times and Rates Extracted from Fitting Procedures for All Molecular Bridges Considered in This Study and Lengths of the Corresponding Gas-Phase Molecules Obtained through DFT Calculations, As Described in the Supporting Information

bridge HS−$[X]_n$−COOH	molecular length (Å)	ET time τ_{ET} (ps)	rate constant k_{ET} (s^{-1})
$[CH_2]_1$	4.0	3 ± 1	3.33×10^{11}
$[CH_2]_3$	6.5	25 ± 2	4.00×10^{10}
$[CH_2]_5$	9.0	225 ± 5	4.44×10^{9}
$[CH_2]_7$	11.5	758 ± 10	1.32×10^{9}
$[C_6H_4]_1$	6.7	2 ± 1	5.00×10^{11}
$[C_6H_4]_2$	11.0	7 ± 2	1.42×10^{11}

experimental time window (0−1100 ps, limited by the length of the optical delay line) was insufficient to clearly resolve the plateau in the OPTP traces (see Figure 2a), increasing the uncertainty in the inferred value for the ET rate (Table 1).

Figure 4 shows the evolution of ET rates as a function of nominal length for bridges (as estimated by DFT, see Table 1

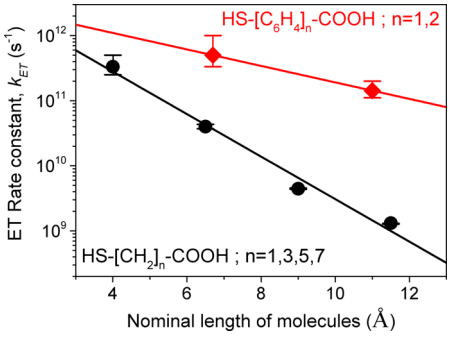

Figure 4. Estimated ET rate constants vs molecular bridge length for *n*-methylene based bridges (HS−$[CH_2]_n$−COOH, with n = 1, 3, 5, 7; black dots) and *n*-phenylene based bridges (HS−$[C_6H_4]_n$−COOH, with n = 1, 2; red squares). Solid lines are best fits to $k_{ET}(d) = k_{ET}(0)\exp[-\beta d]$ as discussed in the text.

and Supporting Information) based on *n*-methylene (HS−$[CH_2]_n$−COOH, n = 1, 3, 5, 7) and *n*-phenylene (HS−$[C_6H_4]_n$−COOH; n = 1, 2) backbones. In the case of *n*-methylene based molecules, the ET rate decays exponentially with bridge length. Indeed, as shown in Figure 4 (black solid line), the data is well-described as a nonresonant coherent tunneling process (where the electron never resides on the bridge; the so-called superexchange mechanism[10,20]) which predicts $k_{ET}(d) = k_{ET}(0)\exp[-\beta d]$, where d is the distance between donor and acceptor states, $k_{ET}(0)$ the ET rate at $d = 0$, and β is the characteristic tunneling decay rate for a given barrier potential (see Figure 1). While the size of the *n*-phenylene data set leaves room for the possibility of ET being dominated by other mechanisms (e.g., electron hopping[10]), we assume here that the charge transfer through the *n*-phenylene based bridges is also mediated by nonresonant coherent tunneling (red solid line in Figure 4), in agreement with reported conductance measurements.[21,22] We obtain for the *n*-phenylene bridges a tunneling decay rate of $\beta = 0.29$ Å^{-1} (or equivalently β_n= 1.25 per phenylene group), while for the *n*-methylene bridges $\beta = 0.75 \pm 0.06$ Å^{-1} (or $\beta_n = 0.94 \pm 0.08$ per methylene group). Within the superexchange model, the tunneling decay rate takes the form $\beta = -(2/a)\ln(H_{bb}/\Delta E_{db})$, where H_{bb} is the internal coupling energy between bridge units, a is the bridge-unit length, and ΔE_{db} is the energy of the mediating tunneling state above the donor ground state. Accordingly, small barrier heights and/or strong bridge unit coupling lead to small β coefficients and large conductance in the donor−bridge−acceptor system. As shown in Figure 5, our

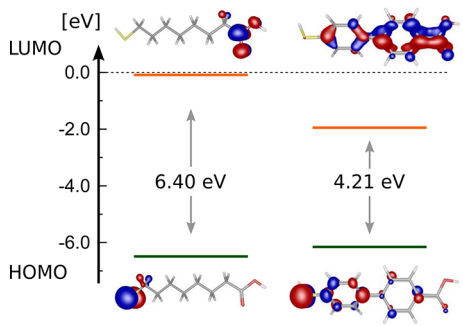

Figure 5. Energetic and spatial distribution of the frontier orbitals of HS−$[CH_2]_7$−COOH (left) and HS−$[C_6H_4]_2$−COOH (right) molecules, calculated using DFT (see the Supporting Information).

theoretical calculations illustrate the origin of the large difference in inferred β's: the *n*-methylene bridges are characterized by highest occupied (HOMO) and lowest unoccupied molecular orbitals (LUMO) strongly localized to either end of the bridge, with a large HOMO−LUMO gap and LUMO level very close to the ionization threshold. The higher-lying virtual orbitals located on the central moiety are similarly weakly coupled. In contrast to the *n*-methylene bridge, the frontier orbitals in the *n*-phenylene molecule delocalize across

dx.doi.org/10.1021/nl402820v | Nano Lett. 2013, 13, 5311−5315

the entire molecule, with both HOMO and LUMO showing significant weight at both ends, and a significantly lower lying LUMO level. This qualitative difference holds true for all linkers employed in this study independent of their length (see the Supporting Information).

Finally, it is worth noting that our obtained β figures agree quantitatively with values reported from conductance measurements through single molecules[21,23] and self-assembled monolayers.[22,24] This agreement strongly supports our results (and methodology) and indicates that conductance and ET rates are indeed closely correlated as theoretically predicted by Nitzan.[25] In conductance measurements the current is measured while varying the DC bias, resulting in $J-V$ curves. The equivalent of varying bias for ET measurements is changing QD size,[6,13,18] which controls the ET driving force ΔG (see Figure 1). Note that β values have been shown to be practically independent of DC bias in molecular conductance measurements,[23] consistent with the notion that in the expression for ET rates $k_{ET}(d) = k_{ET}(0)\ \exp[-\beta d]$, ΔG codetermines the prefactor $k_{ET}(0)$.

In this work we have contributed to clarifying how ET processes are influenced and can be tuned by molecular bridges of different nature and length anchoring QDs to oxide nanoparticles on sensitized systems. For the studied samples, we find that the molecular bridges sandwiched between QD donor and oxide acceptor act as simple resistors to current flow. Similar results have been reported for studies of the tunneling decay rate through an inorganic barrier layer (the shell of a core−shell QD).[26,27] Our findings have implications for the design of QD sensitized solar cells. In these architectures small donor−acceptor energetics (driving forces ΔG, see Figure 1) are desired to enhance potential photoconversion efficiencies.[28] However, small driving forces necessarily imply slow ET rates,[13,18] and then competing relaxation processes within the QDs can quench the output photocurrent in devices. The employment of more conductive molecular bridges (e.g., phenylene vs methylene ones) can counterbalance kinetically that effect and hence improved solar cell efficiencies are in principle within reach. In a complete sensitized solar cell based on a molecular bridge imposing the barrier for current flow between donor and acceptor, we expect that the presence of a hole conducting phase (e.g., electrolyte solution) will likely affect ET rates but not the ET (tunneling) mechanism.

Integrating the concepts of molecular electronics into QDSSCs could further help us choosing functional bridges allowing fast unidirectional ET from donor to acceptor. For example, the employment of molecular bridges showing rectifying behavior between donor and acceptor could potentially prevent back electron recombination from the oxide to the electrolyte or/and from the oxide to the QDs. These recombination pathways are indeed critical for the solar cell performance,[3] and their suppression will result in higher photocurrents and hence efficiencies. Finally, in this work we prove that for given system energetics (ΔG in Figure 1) ET rates in QD sensitized systems can be tuned over several orders of magnitude by appropriate system design.

■ ASSOCIATED CONTENT

Supporting Information

QD synthesis, preparation of QD sensitized SnO_2 films, description of THz-TDS setup and measurements, photooxidation protocol: sample to sample reproducibility and theoretical calculations. This material is available free of charge via the Internet at http://pubs.acs.org.

■ AUTHOR INFORMATION

Corresponding Authors

*E-mail: sachin.kinge@toyota-europe.com.
*E-mail: canovas@mpip-mainz.mpg.de.

Notes

The authors declare no competing financial interest.

■ ACKNOWLEDGMENTS

This work has been financially supported by Toyota Motor Europe NV/SA and by the Max Planck Society. H. Wang is a recipient of a fellowship of the Graduate School Materials Science in Mainz (MAINZ) funded through the German Research Foundation in the Excellence Initiative (GSC 266). The authors acknowledge S. Bohme and A. Houtepen for support on QD synthesis and J. Hunger and S. Parekh for fruitful discussions.

■ REFERENCES

(1) Kamat, P. V. *J. Phys. Chem. C* **2008**, *112*, 18737−18753.
(2) Rühle, S.; Shalom, M.; Zaban, A. *ChemPhysChem* **2010**, *11*, 2290−2304.
(3) Mora-Seró, I.; Bisquert, J. *J. Phys. Chem. Lett.* **2010**, *1*, 3046−3052.
(4) Li, Y.; Zhang, J. Z. *Laser Photonics Rev.* **2010**, *4*, 517−528.
(5) Chen, H. M.; Chen, C. K.; Chang, Y.-C.; Tsai, C.-W.; Liu, R.-S.; Hu, S.-F.; Chang, W.-S.; Chen, K.-H. *Angew. Chem., Int. Ed.* **2010**, *122*, 6102−6105.
(6) Robel, I.; Subramanian, V.; Kuno, M.; Kamat, P. V. *J. Am. Chem. Soc.* **2006**, *128*, 2385−2393.
(7) Dibbell, R. S.; Watson, D. F. *J. Phys. Chem. C* **2009**, *113*, 3139−3149.
(8) Dibbell, R. S.; Youker, D. G.; Watson, D. F. *J. Phys. Chem. C* **2009**, *113*, 18643−18651.
(9) Hyun, B.-R.; Bartnik, A. C.; Sun, L.; Hanrath, T.; Wise, F. W. *Nano Lett.* **2011**, *11*, 2126−2132.
(10) Adams, D. M.; Brus, L.; Chidsey, C. E. D.; Creager, S.; Creutz, C.; Kagan, C. R.; Kamat, P. V.; Lieberman, M.; Lindsay, S.; Marcus, R. A.; Metzger, R. M.; Michel-Beyerle, M. E.; Miller, J. R.; Newton, M. D.; Rolison, D. R.; Sankey, O.; Schanze, K. S.; Yardley, J.; Zhu, X. *J. Phys. Chem. B* **2003**, *107*, 6668−6697.
(11) Watson, D. F. *J. Phys. Chem. Lett.* **2010**, *1*, 2299−2309.
(12) Pijpers, J. J. H.; Koole, R.; Evers, W. H.; Houtepen, A. J.; Boehme, S.; de Mello Donegá, C.; Vanmaekelbergh, D.; Bonn, M. *J. Phys. Chem. C* **2010**, *114*, 18866−18873.
(13) Cánovas, E.; Moll, P.; Jensen, S. A.; Gao, Y.; Houtepen, A. J.; Siebbeles, L. D. A.; Kinge, S.; Bonn, M. *Nano Lett.* **2011**, *11*, 5234−5239.
(14) Ulbricht, R.; Hendry, E.; Shan, J.; Heinz, T. F.; Bonn, M. *Rev. Mod. Phys.* **2011**, *83*, 543−586.
(15) Sykora, M.; Koposov, A. Y.; McGuire, J. A.; Schulze, R. K.; Tretiak, O.; Pietryga, J. M.; Klimov, V. I. *ACS Nano* **2010**, *4*, 2021−2034.
(16) van Sark, W. G. J. H. M.; Frederix, P. L. T. M.; Van den Heuvel, D. J.; Gerritsen, H. C.; Bol, A. A.; van Lingen, J. N. J.; de Mello Donegá, C.; Meijerink, A. *J. Phys. Chem. B* **2001**, *105*, 8281−8284.
(17) Hines, D. A.; Becker, M. A.; Kamat, P. V. *J. Phys. Chem. C* **2012**, *116*, 13452−13457.
(18) Tvrdy, K.; Frantsuzov, P. A.; Kamat, P. V. *Proc. Natl. Acad. Sci. U.S.A.* **2011**, *108*, 29−34.
(19) Jasieniak, J.; Califano, M.; Watkins, S. E. *ACS Nano* **2011**, *5*, 5888−5902.
(20) McConnell, H. M. *J. Chem. Phys.* **1961**, *35*, 8.

(21) Venkataraman, L.; Klare, J. E.; Nuckolls, C.; Hybertsen, M. S.; Steigerwald, M. L. *Nature* **2006**, *442*, 904−907.
(22) Wold, D. J.; Haag, R.; Rampi, M. A.; Frisbie, C. D. *J. Phys. Chem. B* **2002**, *106*, 2813−2816.
(23) Xu, B.; Tao, N. J. *Science* **2003**, *301*, 1221−1223.
(24) Akkerman, H. B.; de Boer, B. *J. Phys.: Condens. Matter* **2008**, *20*, 013001.
(25) Nitzan, A.; Ratner, M. A. *Science* **2003**, *300*, 1384−1389.
(26) Zhu, H.; Song, N.; Lian, T. *J. Am. Chem. Soc.* **2010**, *132*, 15038−15045.
(27) Dworak, L.; Matylitsky, V. V.; Breus, V. V.; Braun, M.; Basché, T.; Wachtveitl, J. *J. Phys. Chem. C* **2011**, *115*, 3949−3955.
(28) Giebink, N. C.; Wiederrecht, G. P.; Wasielewski, M. R.; Forrest, S. R. *Phys. Rev. B* **2011**, *83*, 195326.

dx.doi.org/10.1021/nl402820v | *Nano Lett.* 2013, 13, 5311−5315